Chinese Chemical Letters 36 (2025) 109741

Contents lists available at ScienceDirect

Chinese Chemical Letters

journal homepage: www.elsevier.com/locate/cclet

Designing F-doped Li_3InCl_6 electrolyte with enhanced stability for all-solid-state lithium batteries in a wide voltage window

Ziling Jiang[a,1], Chen Liu[a,1], Jie Yang[a], Xia Li[b,*], Chaochao Wei[a], Qiyue Luo[a], Zhongkai Wu[a], Lin Li[a], Liping Li[c,*], Shijie Cheng[a], Chuang Yu[a,*]

[a] State Key Laboratory of Advanced Electromagnetic Engineering and Technology, School of Electrical and Electronic Engineering, Huazhong University of Science and Technology, Wuhan 430074, China
[b] Innovation Center for Chemical Science, College of Chemistry, Chemical Engineering and Materials Science, Soochow University, Suzhou 215123, China
[c] State Key Laboratory of Inorganic Synthesis and Preparative Chemistry, College of Chemistry, Jilin University, Changchun 130012, China

ARTICLE INFO

Article history:
Received 12 January 2024
Revised 2 February 2024
Accepted 6 March 2024
Available online 8 March 2024

Keywords:
Li_3InCl_6 electrolytes
F-doping
Stability
Electrochemical performance
Solid-state batteries

ABSTRACT

Achieving high energy densities for all-solid-state lithium batteries is restricted by the poor high voltage stability of solid electrolytes. Herein, F-doping strategy is successfully employed on Li_3InCl_6 to obtain enhanced voltage stability and electrode compatability towards bare $LiNi_{0.7}Mn_{0.2}Co_{0.1}O_2$ at high voltages. The optimized $Li_3InCl_{5.5}F_{0.5}$ electrolyte exhibits a decreased conductivity of 1.00 mS/cm, a wider voltage window, and improved electrochemical performance in solid-state batteries when cycled at upper cut-off voltages of 4.5 and 4.8 V (*vs.* Li^+/Li^0). The generation of more stable $LiInF_4$ phase in the cathode mixture of $Li_3InCl_{5.5}F_{0.5}$-based battery ensures superior electrochemical performances compared to the Li_3InCl_6-based battery. The former battery exhibits a higher discharge capacity of 218.9 mAh/g and coulombic efficiency of 86.7% for the first cycle, and retains 80.0% of its original value after 100 cycles when cycled in the range of 3.0–4.5 V (*vs.* Li^+/Li^0). In contrast, the Li_3InCl_6-based battery exhibits lower capacities and faster degradation under the same conditions due to the formation of $InCl_3$ phase with poor electrochemical stability. This work facilitates the advancement of high energy density solid-state battery technologies by utilizing high-voltage cathodes.

With the introduction of China's dual carbon policy, there is a growing demand for electrified vehicles and scalable energy storage. Nevertheless, conventional liquid-state lithium battery systems pose safety hazards, and their energy density has essentially reached its limit. All solid-state lithium batteries (ASSLBs), offering both higher safety and energy density, as well as extended cycle life, hold the potential to fundamentally address these issues. As it is widely acknowledged, raising the upper cut-off charging voltage is a crucial method to drive the advancement of high-energy-density ASSLBs [1–8]. Therefore, to achieve high energy density in ASSLBs, it is crucial to develop solid-state electrolytes (SSEs) that are stable at high voltages [9–12]. These SSEs should possess a wide electrochemical stability window (ESW) with a high oxidation potential exceeding 4.2 V (*vs.* Li^+/Li^0).

In currently reported electrolytes, oxide electrolytes have demonstrated their potential for high oxidation potentials, exceeding 5.0 V (*vs.* Li^+/Li^0), making them compatible with high-voltage cathodes in high-energy-density applications [13,14]. However, their intrinsic rigidity often leads to poor electrode/electrolyte interface contact. Sulfide solid electrolytes garner significant attention owing to their exceptionally high ionic conductivity and ease of mechanical processing. Nevertheless, their limited ESW within the range of 1.5–2.5 V (*vs.* Li^+/Li^0) is also considered a primary obstacle to their utilization in high-voltage ASSLBs. Direct contact between sulfide electrolytes and layered oxide cathodes results in substantial interfacial resistance due to inevitable side reactions [15–19]. Additionally, the interfacial resistance is exacerbated by the solid electrolyte's decomposition under high voltage.

In recent years, halide electrolytes have emerged as newcomers in the field and have shown promising developments. Advanced halide solid electrolytes (*e.g.*, Li_3InCl_6, Li_3ErCl_6, $Li_2Sc_{2/3}Cl_4$) have achieved Li-ion conductivity values exceeding 1 mS/cm at room temperature [20–26]. Ma *et al.* have designed even lower-cost solid electrolytes such as $Li_{1.75}ZrCl_{4.75}O_{0.5}$ with Li-ion conductivity as

* Corresponding authors.
E-mail addresses: cyu2020@hust.edu.cn (X. Li), xiali@suda.edu.cn (L. Li), lipingli@jlu.edu.cn (C. Yu).
[1] These authors contributed equally to this work.

https://doi.org/10.1016/j.cclet.2024.109741
1001-8417/

high as 2.42 mS/cm [27]. Additionally, halide electrolytes, such as chloride-based electrolytes, exhibit a relatively high theoretical potential of up to 4.2 V (*vs.* Li^+/Li^0). Asano *et al.* reported a Li_3YCl_6 SSE with a wide ESW of 0.62–4.21 V (*vs.* Li^+/Li^0) [28]. However, these compounds are still inadequate for the application in ASSLBs at higher voltages. The oxidation of lithium chloride electrolyte occurs above 4.3 V, resulting in the formation of lithium-deficient metal chloride products, such as YCl_3, $InCl_3$, and $ErCl_3$ [29,30]. These products lack sufficient Li^+ conduction pathways, leading to continuous consumption of the SSEs and thereby reduces the overall battery performance. According to Mo *et al.*'s simulation results, fluoride-based SSEs exhibit the highest oxidation stability potential compared to other halide-based SSEs [29]. However, the strong electronegativity of fluorine (F) yields a relatively lower Li-ion conductivity.

In this work, partially substitution of Cl^- with F^- in the Li_3InCl_6 structure was employed to achieve acceptable Li-ion conductivity and high oxidation stability for the construction of high-voltage ASSLBs. The optimized $Li_3InCl_{5.5}F_{0.5}$ electrolyte demonstrates enhanced voltage stability, exceeding 4.5 V (*vs.* Li^+/Li^0). ASSLBs consisiting of the bare $LiNi_{0.7}Mn_{0.2}Co_{0.1}O_2$ and $Li_3InCl_{5.5}F_{0.5}$ electrolyte show superior electrochemical performance under upper cut-off voltages of 4.5 and 4.8 V (*vs.* Li^+/Li^0). Multiple characterizations were combined to further elucidate the working mechanism. This work proposes a strategy for designing high-voltage stable solid electrolytes for ASSLBs with high energy density.

To prepare the series of F-doped Li_3InCl_6 electrolytes, the mixture of starting materials (LiCl, $InCl_3$, and InF_3) was first ball-milled and followed by a heat treatment process to promote the crystallinity and Li-ion conductivities of the obtained materials. The primary diffraction peaks of the synthesized $Li_3InCl_{6-x}F_x$ materials are well matched to the pure Li_3InCl_6 phase with a monoclinic phase (Fig. 1a). XRD refinements were conducted on $Li_3InCl_{5.5}F_{0.5}$ to elucidate structural distinctions. Fig. 1b displays the measured XRD patterns and their fits, demonstrating a good agreement with the simulated XRD peaks. The corresponding crystal structure is shown in Fig. 1c, and the relevant parameters obtained from the refinements can be found in Table S1 (Supporting information).The total resistances of the $Li_3InCl_{6-x}F_x$ (x = 0, 0.3, 0.5, 0.7, and 0.9) materials decrease with increasing F^- dopant amounts (Fig. 1d), indicating that F^- doping strategy reduces Li-ion conductivity of the Li_3InCl_6 electrolyte. The room temperature Li-ion conductivities deduced from the resistance results are 1.40 mS/cm for Li_3InCl_6, 1.17 mS/cm for $Li_3InCl_{5.7}F_{0.3}$, 1.00 mS/cm for $Li_3InCl_{5.5}F_{0.5}$, 0.95 mS/cm for $Li_3InCl_{5.3}F_{0.7}$, and 0.48 mS/cm for $Li_3InCl_{5.1}F_{0.9}$, respectively (Fig. 1e). An obvious drops in Li-ion conductivities is observd as the dopant amount increases from x = 0.7 to x = 0.9, which aligns well with the XRD results that the intensity of the major diffraction peaks of the pure phase of Li_3InCl_6 experiences a sharp decline. Further Li-ion conductivities of these prepared samples under the selected temperatures were also confirmed that ionic conductivities decrease with increasing F^- amount in the structure in Fig. 1f. Considering the ionic conductivity of different compositions, $Li_3InCl_{5.5}F_{0.5}$ with an acceptable Li-ion conductivity of 1.00 mS/cm was chosen as the target SSE in this study. Electronic conductivity changes of Li_3InCl_6 electrolyte before and after introducing F^- was also investigated. (Fig. 1g) Finally, electrochemical stability of $Li_3InCl_{5.5}F_{0.5}$ electrolytes was also studied using the typical characterization method as reported [24]. As depicted in Fig. 1h, the $Li_3InCl_{5.5}F_{0.5}$ electrolyte exhibits superior voltage stability comapred to the bare Li_3InCl_6 electrolyte (around 4 V *vs.* Li^+/Li^0) with a high stable potential over 4.5 V (*vs.* Li^+/Li^0). To investigate the electrochemical performance of the electrolytes, ASSLBs consiting of the bare $LiNi_{0.7}Mn_{0.2}Co_{0.1}O_2$ and $Li_3InCl_6/Li_3InCl_{5.5}F_{0.5}$ electrolytes were assembled and cycled within the voltage range of 3.0–4.5 V (*vs.* Li^+/Li^0).

To validate the improved electrochemical stability of F-doped Li_3InCl_6 electrolytes, the bare $LiNi_{0.7}Mn_{0.2}Co_{0.1}O_2$ was selected as the cathode active material combined with the pristine Li_3InCl_6 and $Li_3InCl_{5.5}F_{0.5}$ electrolytes and Li-In anode to assemble all-solid-state lithium batteries. To aviod interfacail instability between the halide electrolytes and Li-In anode in the batteries, a thin layer of $Li_{5.5}PS_{4.5}Cl_{1.5}$ electrolyte was added to isolate the direct contact [31]. Therefore, three types of batteries configurations, $LiNi_{0.7}Mn_{0.2}Co_{0.1}O_2/Li_{5.5}PS_{4.5}Cl_{1.5}$/Li-In, $LiNi_{0.7}Mn_{0.2}Co_{0.1}O_2$-$Li_3InCl_6/Li_3InCl_6/Li_{5.5}PS_{4.5}Cl_{1.5}$/Li-In, and $LiNi_{0.7}Mn_{0.2}Co_{0.1}O_2$-$Li_3InCl_{5.5}F_{0.5}/Li_3InCl_{5.5}F_{0.5}/Li_{5.5}PS_{4.5}Cl_{1.5}$/Li-In were constructed in this work. These batteries were cycled with a wide charge/discharge voltage range of 2.4–3.9 V (*vs.* Li-In, equivelent to 3.0–4.5 V *vs.* Li^+/Li^0) to assess their electrochemical stability. When cycled at 0.1 C, the $LiNi_{0.7}Mn_{0.2}Co_{0.1}O_2/Li_{5.5}PS_{4.5}Cl_{1.5}$/Li-In battery delivers an initial discharge capacity of 157.9 mAh/g with a coulombic efficiency of 69.19%, while these values for the $LiNi_{0.7}Mn_{0.2}Co_{0.1}O_2$-$Li_3InCl_6/Li_3InCl_6/Li_{5.5}PS_{4.5}Cl_{1.5}$/Li-In battery are 187.6 mAh/g and 77.97%, and for the $LiNi_{0.7}Mn_{0.2}Co_{0.1}O_2$-$Li_3InCl_{5.5}F_{0.5}/Li_3InCl_{5.5}F_{0.5}/Li_{5.5}PS_{4.5}Cl_{1.5}$/Li-In battery are 218.9 mAh/g and 86.68%. The $LiNi_{0.7}Mn_{0.2}Co_{0.1}O_2$-$Li_3InCl_6$ cathode mixture displays greater initial discharge capacity and coulombic efficiency compared to the $LiNi_{0.7}Mn_{0.2}Co_{0.1}O_2$-$Li_{5.5}PS_{4.5}Cl_{1.5}$. This is due to the superior interfacail stability of the Li_3InCl_6 electrolyte than the $Li_{5.5}PS_{4.5}Cl_{1.5}$ electrolyte. Sulfide electrolytes are known to undergo serious side reactions and space charge effects towards the bare layered cathode materials in a typical charge/discharge [32–34]. Replacing sulfide electrolytes in the cathode mixture with lithium halide electrolytes can significantly increase capacities and coulombic efficiencies during the first few cycles [35]. When zooming in on the charge/discharge voltage window, the side reaction effects become worse due to the degradation of sulfide electrolytes at a higher upper cut-off voltage of 4.5 V (*vs.* Li^+/Li^0) in this work. Based on the LSV test results shown in Fig. 1h, $Li_3InCl_{5.5}F_{0.5}$ exhibits superior voltage stability compared to bare Li_3InCl_6. This indicates that the $Li_3InCl_{5.5}F_{0.5}$ electrolyte may result in higher capacity and coulombic efficiencies in solid-state batteries. This assumption is supported by our battery performance results presented in Fig. 2. The fabricated $LiNi_{0.7}Mn_{0.2}Co_{0.1}O_2$-$Li_3InCl_{5.5}F_{0.5}/Li_3InCl_{5.5}F_{0.5}/Li_{5.5}PS_{4.5}Cl_{1.5}$/Li-In battery delivers the highest discharge capacity and Coulombic efficiency values among these three battery configurations in Fig. 2a. Moreover, the electrode polarizations of the cathode mixtures decrease in the sequence of $LiNi_{0.7}Mn_{0.2}Co_{0.1}O_2$-$Li_3InCl_{5.5}F_{0.5}$, $LiNi_{0.7}Mn_{0.2}Co_{0.1}O_2$-$Li_3InCl_6$, and $LiNi_{0.7}Mn_{0.2}Co_{0.1}O_2$-$Li_{5.5}PS_{4.5}Cl_{1.5}$ mixtures, which are due to the electrochemical stability of different solid electrolyte when cycled with the bare $LiNi_{0.7}Mn_{0.2}Co_{0.1}O_2$ active material in a high cut-off voltage. During the subsequent cycling tests, the $LiNi_{0.7}Mn_{0.2}Co_{0.1}O_2/Li_{5.5}PS_{4.5}Cl_{1.5}$/Li-In battery exhibits a rapid decline in discharge capacities and can only retain 27.0% of its initial discharge capacity with a value of 42.7 mAh/g after 100 cycles. In contrast, the $LiNi_{0.7}Mn_{0.2}Co_{0.1}O_2$-$Li_3InCl_6/Li_3InCl_6/Li_{5.5}PS_{4.5}Cl_{1.5}$/Li-In battery demonstrates much higher discharge capacities and maintains 52.5% of its original value, with a discharge capacity of 98.4 mAh/g for the 100th cycle. While the assembled $LiNi_{0.7}Mn_{0.2}Co_{0.1}O_2$-$Li_3InCl_{5.5}F_{0.5}/Li_3InCl_{5.5}F_{0.5}/Li_{5.5}PS_{4.5}Cl_{1.5}$/Li-In battery exhibits the best cycling performance among these three batteries. Specifically, it provides a discharge capacity of 175.1 mAh/g after 100 cycles with a capacity retention of 80.0%. The solid-state lithium batteries that contain $Li_3InCl_{5.5}F_{0.5}$ electrolytes in both the cathode mixture layer and solid electrolyte layer demonstrate the highest discharge capacity retention among these batteries. Furthermore, the dQ/dV plots of these different cathodes based on the charge/discharge curves in Fig. 2b were also performed. These curves depict characteristic oxidation–

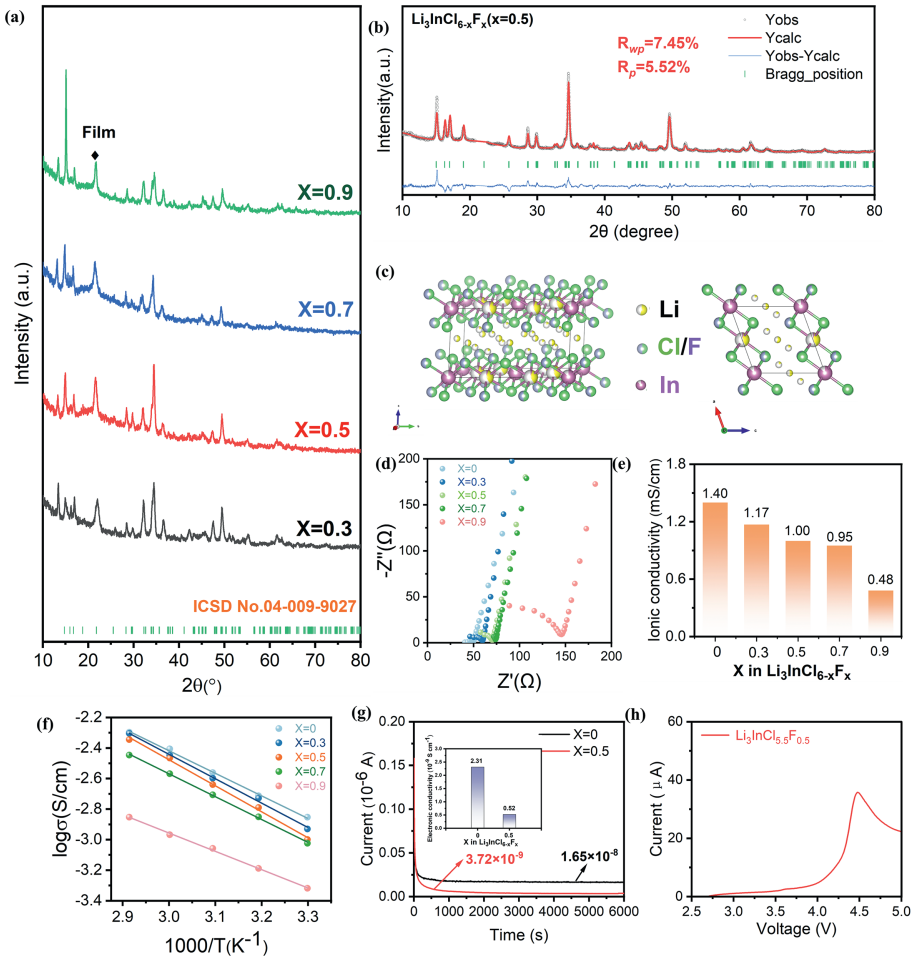

Fig. 1. (a) XRD patterns of the prepared $Li_3InCl_{6-x}F_x$ (x = 0.3, 0.5, 0.7, and 0.9) materials. (b) XRD refinement patterns of the $Li_3InCl_{5.5}F_{0.5}$. (c) Crystal structures of the chosen unit cells for the $Li_3InCl_{5.5}F_{0.5}$. (d) Room temperature impedance spectra and (e) corresponding Li-ion conductivities of these $Li_3InCl_{6-x}F_x$ (x = 0, 0.3, 0.5, 0.7, and 0.9) electrolytes. (f) The Arrhenius plots deduced from Li-ion conductivities of these different compositions measured at various temperatures. (g) RT electronic conductivities measured with the potentiostatic polarization method of the Li_3InCl_6 and $Li_3InCl_{5.5}F_{0.5}$ electrolytes. (h) the LSVcurves of the designed battery configuration of using solid electrolyte-carbon composite and Li electrodes for the obtained $Li_3InCl_{5.5}F_{0.5}$ electrolytes.

reduction peaks corresponding to various phase transitions during the processes of lithiation and delithiation. As illustrated in Fig. 2c, the oxidation/reduction peaks of the electrode based on $LiNi_{0.7}Mn_{0.2}Co_{0.1}O_2$-$Li_3InCl_{5.5}F_{0.5}$ highly overlap in different cycles. For the $LiNi_{0.7}Mn_{0.2}Co_{0.1}O_2$-$Li_3InCl_6$ electrode, at the 50th cycle, the distinct oxidation peak at 3.65 V and the corresponding reduction peak at 3.56 V disappeared, indicating an irreversible phase transition. This is likely the cause of the sudden and severe capacity decay (Fig. 2d). In addition, based on $LiNi_{0.7}Mn_{0.2}Co_{0.1}O_2$-$Li_{5.5}PS_{4.5}Cl_{1.5}$ electrode, the dQ/dV curve at the 100th cycle exhibits oxidation/reduction peaks that are broader and much lower in intensity compared to the corresponding peaks in the first cycle curve, indicating a deterioration in the reversibility of lithiation (Fig. 2e). The Nyquist plots of the three battery configurations before and after 100 cycles are shown in Figs. 2f-h. The changes in EIS spectra for the three batteries are primarily concentrated in the low-frequency region, as opposed to the high-frequency region. The equivalent circuits were employed to analyze all nyquist plots (Figs. S2 and S3 in Supporting information). In terms of the fitting outcomes outlined in Table S2 (Supporting information), the values of R_{ct2} are the highest for all three battery configurations. This indicates that the primary contributor to the increase in impedance is the interfacial resistance between the Ni-rich layered oxide and the electrolyteHG. This aligns with findings reported in other relevant studies [36–39]. Additionally, by comparing the R_{ct2} values of the three configurations, the battery based on $Li_3InCl_{5.5}F_{0.5}$ exhibits the smallest R_{ct2} value after 100 cycles compared to the other two batteries, implying that $Li_3InCl_{5.5}F_{0.5}$ can enhance interfacial stability and possess better high-voltage tolerance. Furthermore, electrochemical performances of these batteries at a higher C-rate of 0.5 C within the same voltage window were also examined. The $LiNi_{0.7}Mn_{0.2}Co_{0.1}O_2$-$Li_3InCl_{5.5}F_{0.5}$ cathode shows higher discharge capacities and smaller electrode polarizations for the selected cycles compared to the $LiNi_{0.7}Mn_{0.2}Co_{0.1}O_2$-$Li_3InCl_6$ and $LiNi_{0.7}Mn_{0.2}Co_{0.1}O_2$-$Li_{5.5}PS_{4.5}Cl_{1.5}$ cathodes (Fig. 2i). All batteries exhibit good cycling performances when charged/discharged at 0.5 C (Fig. 2j), while these cathode mixtures contain lithium halide electrolytes (Li_3InCl_6 and $Li_3InCl_{5.5}F_{0.5}$) demonstrate markedly higher discharge capacities compared to the $LiNi_{0.7}Mn_{0.2}Co_{0.1}O_2$-$Li_{5.5}PS_{4.5}Cl_{1.5}$ cathode during cycling. The latter cathode exhibits discharge capacities of 95.3 mAh/g and 86.4 mAh/g for the 1st and 80th cycles when cycled at 0.5 C, respectively. In comparision, the $LiNi_{0.7}Mn_{0.2}Co_{0.1}O_2$-$Li_3InCl_6$ cathode shows much higher discharge capacities of 169.5 mAh/g for the first cycle and 156.3 mAh/g for the 80th cycle, and the $LiNi_{0.7}Mn_{0.2}Co_{0.1}O_2$-$Li_3InCl_{5.5}F_{0.5}$ cathode demonstrates even higher discharge capacities of 180.9 mAh/g at the beginning and 172.1 mAh/g after 80 cycles. The cathodes consisting of lithium halide electrolytes exhibit superior capacities compared to those using sulfide electrolytes due to better voltage stability at higher voltages and excellent interfacial sta-

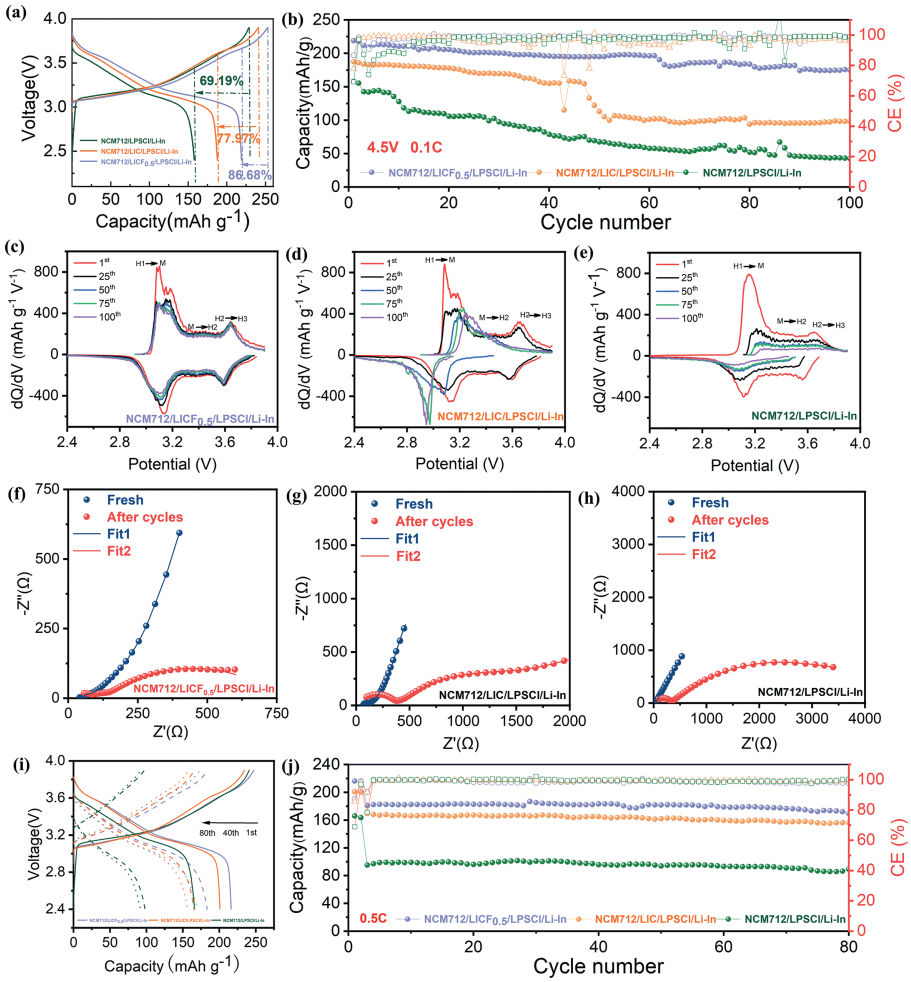

Fig. 2. (a) The initial charge/discharge curves of the assembled $LiNi_{0.7}Mn_{0.2}Co_{0.1}O_2/Li_{5.5}PS_{4.5}Cl_{1.5}$/Li-In, $LiNi_{0.7}Mn_{0.2}Co_{0.1}O_2$-$Li_3InCl_6/Li_3InCl_6/Li_{5.5}PS_{4.5}Cl_{1.5}$/Li-In, and $LiNi_{0.7}Mn_{0.2}Co_{0.1}O_2$-$Li_3InCl_{5.5}F_{0.5}/Li_3InCl_{5.5}F_{0.5}/Li_{5.5}PS_{4.5}Cl_{1.5}$/Li-In batteries when cycled at 0.1 C between 2.4 V and 3.9 V (*vs.* Li-In, 3.0–4.5 V *vs.* Li^+/Li^0) at r.t. (b) The corresponding cycling performances of these batteries at the selected C-rate. (c-e) The d*Q*/d*V* cruve changes obtained based on the chagre/dischagre profiles of different battery configurations when cycled at 0.1 C under RT in (b). (f-h) EIS spectra of these batteries before and after 100 cycles at 0.1 C. (i) Charge/discahrge profiles of the chosen cycles and (j) the cycling performances of these ASSLBs with a higher C-rate of 0.5 C.

bility with bare high nickel layered active materials, such as $LiNi_{0.7}Mn_{0.2}Co_{0.1}O_2$. Our previous research found that the interfacail instability between Li_3InCl_6 and $Li_{5.5}PS_{4.5}Cl_{1.5}$ electrolytes yields poor electrochemical performance for the corresponding batteries [16]. The improved battery performance of the $Li_3InCl_{5.5}F_{0.5}$-based solid-state battery, compared to the Li_3InCl_6-based battery, is attributed to the enhanced interfacial stability between the halide and $Li_{5.5}PS_{4.5}Cl_{1.5}$ electrolytes resulting from F-doping.

The rate capabilities of the above battery configurations were further studied to reveal the effect of F-doping on electrochemcial performances at higher cycling current densities under room temperature. All batteries were charged/discharged at these chosen C-rates of 0.1, 0.2, 0.5, 1.0, and 2.0 C between 2.4 V and 3.9 V (*vs.* Li-In). As illustrated in Figs. 3a-c, the $LiNi_{0.7}Mn_{0.2}Co_{0.1}O_2$-$Li_3InCl_{5.5}F_{0.5}$ cathode shows higher discharge capacities and smaller electrode polarizations compared to the other two cathodes, $LiNi_{0.7}Mn_{0.2}Co_{0.1}O_2$-$Li_3InCl_6$ and $LiNi_{0.7}Mn_{0.2}Co_{0.1}O_2$-$Li_{5.5}PS_{4.5}Cl_{1.5}$, when cycled at these chosen C-rates. When the charge/discharge C-rates increase step-by-step from 0.1 C to 2.0 C, and then recover back to 0.1 C, the $LiNi_{0.7}Mn_{0.2}Co_{0.1}O_2$-$Li_{5.5}PS_{4.5}Cl_{1.5}$ cathode delivers dsicharge capacities of 171.8, 143.9, 92.1, 38.1, 2.2, and 169.1 mAh/g, respectively. In contrast, the $LiNi_{0.7}Mn_{0.2}Co_{0.1}O_2$-$Li_3InCl_6$ cathode shows much higher corresponding discharge capacity values of 198.0, 179.3, 162.6, 139.1, 99.4, and 181.9 mAh/g, respectively. Whereas the $LiNi_{0.7}Mn_{0.2}Co_{0.1}O_2$-$Li_3InCl_{5.5}F_{0.5}$ cathode diplays the highest discharge capacities at the same C-rates among these batteries, 222.3, 204.8, 182.3, 157.0, 120.2, and 209.7 mAh/g, respectively. Moreover, cycling performance results in Fig. 3d also confirm the conclusion that the solid-state battery utilizing $Li_3InCl_{5.5}F_{0.5}$ electrolyte exhibits the best rate capability. To further verify the improved voltage stability of Li_3InCl_6 electrolyte after F-doping, the Li_3InCl_6-based and $Li_3InCl_{5.5}F_{0.5}$-based ASSLBs were also cycled at 0.5 C with an even higher upper cut-off voltage of 4.2 V (*vs.* Li-In, corresponding to 4.8 V *vs.* Li^+/Li^0) at RT. The Li_3InCl_6-based battery demonstrates similar chagre/discharge profiles with comparable voltage plateau differences at the beginning when compared to the $Li_3InCl_{5.5}F_{0.5}$-based battery (Fig. 3e). With cycling goes on, the latter delivers much higher discharge capacities and smaller electrode polarizations for the chosen cycles (20^{th}, 40^{th}, 80^{th}). The corresponding d*Q*/d*V* curves obtained from the charge/discharge curves in Figs. 3f and g exhibit the same conclusion. These d*Q*/d*V* peaks observed for the $Li_3InCl_{5.5}F_{0.5}$-based battery are highly overlaped each other for different cycles (Fig. 3f), whereas these peaks for the Li_3InCl_6-based battery exhibit clear intensity decay in Fig. 3g, indicating a fast degradation of discharge capacities during cycling. After 80 cycles within the range

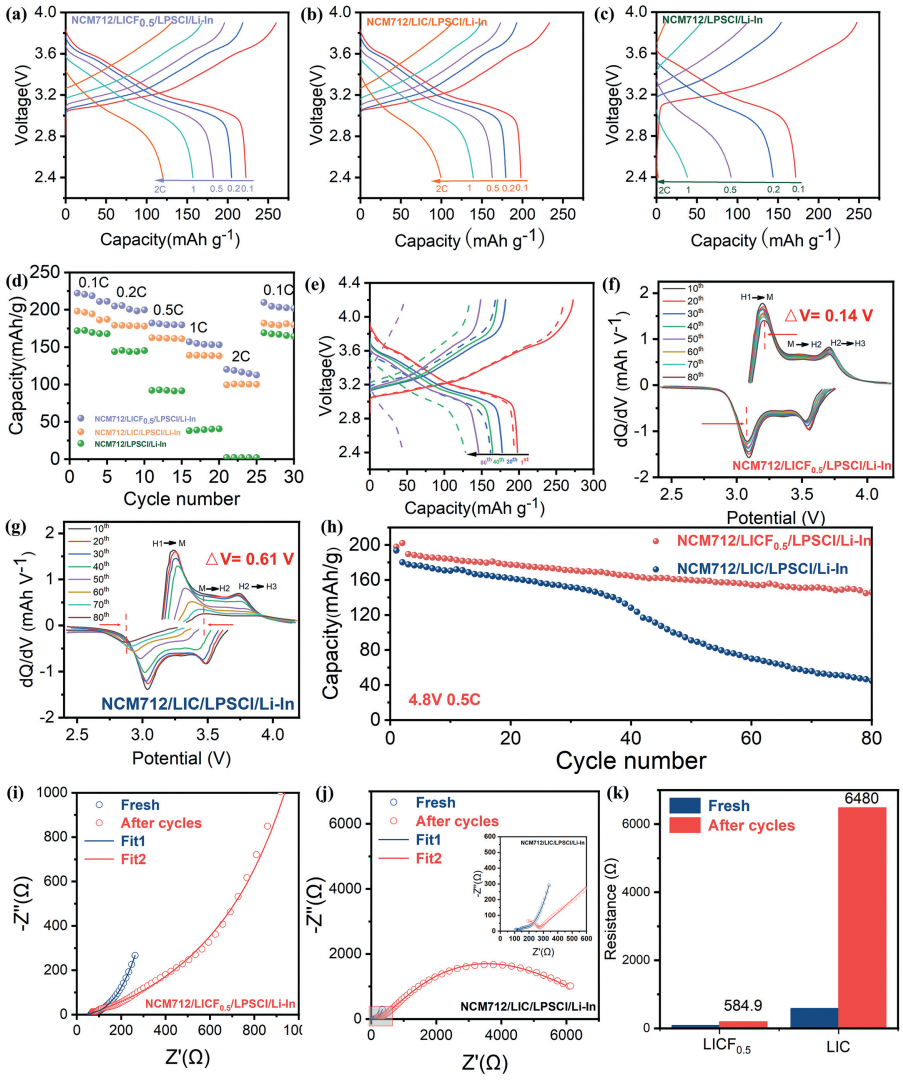

Fig. 3. (a-c) Initial charge/discharge curves of the fabricated $LiNi_{0.7}Mn_{0.2}Co_{0.1}O_2$/$Li_{5.5}PS_{4.5}Cl_{1.5}$/Li-In, $LiNi_{0.7}Mn_{0.2}Co_{0.1}O_2$-$Li_3InCl_6$/$Li_3InCl_6$/$Li_{5.5}PS_{4.5}Cl_{1.5}$/Li-In, and $LiNi_{0.7}Mn_{0.2}Co_{0.1}O_2$-$Li_3InCl_{5.5}F_{0.5}$/$Li_3InCl_{5.5}F_{0.5}$/$Li_{5.5}PS_{4.5}Cl_{1.5}$/Li-In batteries when cycled at different C-rates between 2.4 V and 3.9 V (*vs.* Li-In, 3.0–4.5 V *vs.* Li^+/Li^0) at room temperature. (d) Rate capability tests of these different battery configurations. (e) The charge/discharge profiles and (h) corresponding cycling performances of the $LiNi_{0.7}Mn_{0.2}Co_{0.1}O_2$-$Li_3InCl_6$/$Li_3InCl_6$/$Li_{5.5}PS_{4.5}Cl_{1.5}$/Li-In and $LiNi_{0.7}Mn_{0.2}Co_{0.1}O_2$-$Li_3InCl_{5.5}F_{0.5}$/$Li_3InCl_{5.5}F_{0.5}$/$Li_{5.5}PS_{4.5}Cl_{1.5}$/Li-In batteries when cycled at 0.5 C between 2.4 V and 4.2 V (*vs.* Li-In, 3.0–4.8 V *vs.* Li^+/Li^0). (f, g) The d*Q*/d*V* cruve changes obtained based on the chagre/dischagre profiles of different battery configurations in (h). (i-k) Nyquist plots and the fitting results of these two batteries before and after cycling.

of 3.0–4.8 V (*vs.* Li^+/Li^0), compared with the $LiNi_{0.7}Mn_{0.2}Co_{0.1}O_2$-$Li_3InCl_6$ electrode, the $LiNi_{0.7}Mn_{0.2}Co_{0.1}O_2$-$Li_3InCl_{5.5}F_{0.5}$ electrode exhibits a much smaller voltage gap between the oxidation and reduction peaks (0.14 V *vs.* 0.61 V). This agrees well with the following cycling performance of these batteries in Fig. 3h. Compared to the $Li_3InCl_{5.5}F_{0.5}$-based battery, the Li_3InCl_6-based battery shows slightly lower discharge capacities during the first 40 cycles, and then delivers much lower discharge capacities in the subsequent 40 cycles. Specicallly, the Li_3InCl_6-based battery delivers a dischagre capacity of 177.8 mAh/g for the 3rd cycle, and suffers a fast capacity degradation in the following 77 cycles and sustains a dischagre capacity of 44.8 mAh/g for the 80th cycle with a capacity retention of 25.2%. For comparison, the $Li_3InCl_{5.5}F_{0.5}$-based battery shows discharge capacities of 189.4 mAh/g and 145.9 mAh/g for the corresponding 3rd and 80th cycles with a much higher capacity retention of 77.0%. The higher capacities and superior cyclability of the $Li_3InCl_{5.5}F_{0.5}$-based battery compared to the Li_3InCl_6-based battery is attributed to the enhanced electrochemical stability after introducing F^- in the structure of Li_3InCl_6 electrolyte when cycled at an ultrahigh upper cut-off voltage (4.8 V *vs.* Li^+/Li^0). This result is consistent with previous battery performance depicted in Fig. 2b. EIS was further performed on both battery configurations before and after 80 cycles to reveal the resistance variations. As illustrated in Figs. 3i-k, the Li_3InCl_6-based battery experiences a notable rise in overall resistance, peaking at 6480 Ω after 80 cycles. In contrast, the $Li_3InCl_{5.5}F_{0.5}$-based battery shows a smaller total resistance during the same cycling process, remaining at 584.9 Ω. Table S3 (Supporting information) lists the specific numerical values of the fitted impedances for each component. Due to the decreased electrochemical stability of Li_3InCl_6 electrolyte at 4.8 V (*vs.* Li^+/Li^0), these side reaction products caused by Li_3InCl_6 and $LiNi_{0.7}Mn_{0.2}Co_{0.1}O_2$ in the cathode mixture result in a large interfacail resistance, as detected in Fig. 3k. In contrast, $Li_3InCl_{5.5}F_{0.5}$ electrolyte with higher electrochemical stability shows excellent interface stability with the bare $LiNi_{0.7}Mn_{0.2}Co_{0.1}O_2$ when cycled at 4.8 V (*vs.* Li^+/Li^0), leading to a much smaller resistances for the corresponding battery.

Finally, structural changes of the $LiNi_{0.7}Mn_{0.2}Co_{0.1}O_2$ particles after cycling with the Li_3InCl_6 and $Li_3InCl_{5.5}F_{0.5}$ electrolytes with a charge/discharge voltage window of 3.0 and 4.5 V (*vs.*

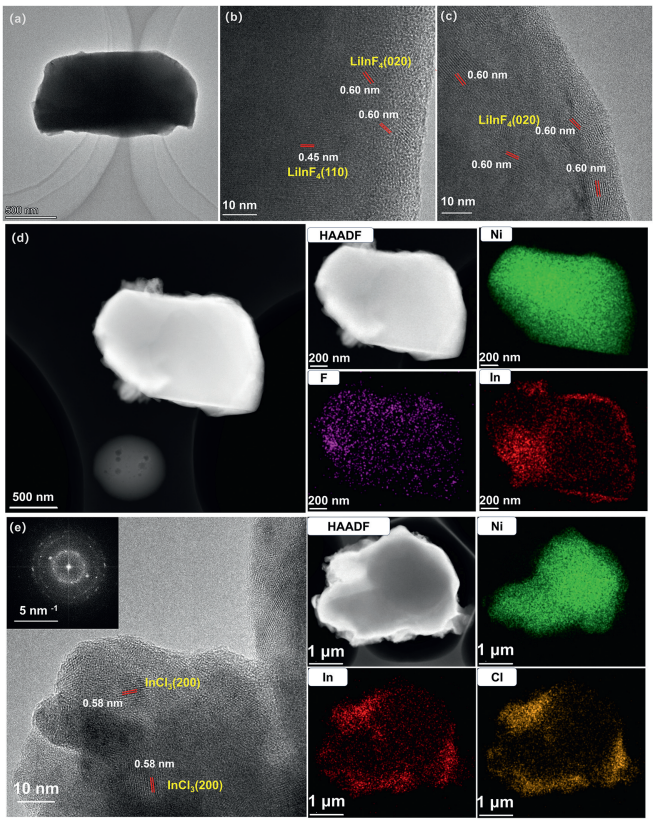

Fig. 4. (a) Bright-field STEM image and (b, c) the corresponding selected area electron diffraction patterns of $LiNi_{0.7}Mn_{0.2}Co_{0.1}O_2$ active material cycled with the $Li_3InCl_{5.5}F_{0.5}$ electrolyte after 100 cycles at 0.1 C in ASSLBs. (d) TEM image and EDS mapping of different elements (Ni, F, and In) of the cycled $LiNi_{0.7}Mn_{0.2}Co_{0.1}O_2$ particle. (e) High-resolution TEM image of the $LiNi_{0.7}Mn_{0.2}Co_{0.1}O_2$ cycled with the Li_3InCl_6 electrolyte and EDS mapping of Ni, In, and Cl elements of the chosen cycled particle. The inset figure is the electron diffraction patterns of the chosen area.

Li^+/Li^0) were also explored *via ex-situ* TEM. As shown in Fig. 4a, $LiNi_{0.7}Mn_{0.2}Co_{0.1}O_2$ particles maintained their particle integrity after cycling with the F-modified Li_3InCl_6 electrolyte. Additionally, well-defined lattice fringes with values of 0.45 and 0.60 nm which belonging to the $LiInF_4$ phase are also detected in the image, suggesting the generation of $LiInF_4$ during cycling in the cathode mixture (Figs. 4b and c). The uniform distribution of materials containing F and In at the edges of the selected particles is affirmed by the EDX mapping results (Fig. 4d). Previous reseach reported that $LiInF_4$ possesses a wide stable volatge window with a high upper cut-off voltage exceed 6.0 V (*vs.* Li^+/Li^0) [40]. The formation of a small amount of $LiInF_4$ phase can enhance the electrochemical stability and increase the intrinsic thermodynamic stability limitation of $Li_3InCl_{5.5}F_{0.5}$ electrolyte. This leads to a zoomed charge/discharge voltage window and mitigates the side reaction between the bare $LiNi_{0.7}Mn_{0.2}Co_{0.1}O_2$ and $Li_3InCl_{5.5}F_{0.5}$ under higher upper cut-off voltages, such as 4.5 and 4.8 V (*vs.* Li^+/Li^0). This analysis is consistent with previous calculation results [40,41]. In comparison, the partcile integrity of $LiNi_{0.7}Mn_{0.2}Co_{0.1}O_2$ is also remained after cycled with the bare Li_3InCl_6 electrolyte when cycled at 4.5 (*vs.* Li^+/Li^0), whereas the lattice fring of 0.58 nm assigned to the $InCl_3$ is observed in Fig. 4e, indicating the formation of $InCl_3$ phase in the $LiNi_{0.7}Mn_{0.2}Co_{0.1}O_2$-$Li_3InCl_6$ cathode mixture. However, the $InCl_3$ phase exhibits poor stability under high voltage as reported [42]. Therefore, intense side reactions occur between the bare $LiNi_{0.7}Mn_{0.2}Co_{0.1}O_2$ and Li_3InCl_6 under 4.5 and 4.8 V (*vs.* Li^+/Li^0) in the cathode mixture when the corresponding battery worked at these high upper cut-off voltage, leading to poor battery performances (Figs. 2b and 3h).

In summary, we have successfully designed F-doped Li_3InCl_6 electrolyte with comparable conductivity and enhanced electrochemical stability. By tuning the F^- dopant in the structure, the optimal electrolyte with a composition of $Li_3InCl_{5.5}F_{0.5}$ exhibits a RT Li-ion conductivity of 1.00 mS/cm and improved electrochemcial compatability towards bare $LiNi_{0.7}Mn_{0.2}Co_{0.1}O_2$ active materials under 4.5 and 4.8 V (*vs.* Li^+/Li^0). Therefore, the $Li_3InCl_{5.5}F_{0.5}$-based solid-state battery demonstrates superior charge/discharge capacities and coulombic efficiencies, rate capability, and cycling performance in comparison to the $Li_{5.5}PS_{4.5}Cl_{1.5}$-based and Li_3InCl_6-based batteries under the same testing conditions. The $Li_{5.5}PS_{4.5}Cl_{1.5}$-based battery exhibits rapid capacity decay due to intense side ractions between the sulfide electrolyte and high-nickel active materials. The battery initially provides a discharge capacity of 157.9 mAh/g and retains 27.0% of its capacity after 100 cycles at 0.1 C between 3.0 V and 4.5 V (*vs.* Li^+/Li^0). In comparision, these values are 187.6 mAh/g and 52.5% for the Li_3InCl_6-based battery, and 218.9 mAh/g and 80.0% for the $Li_3InCl_{5.5}F_{0.5}$-based battery, respectively. EIS results confirm that the differences in battery performance are closely related to the interfacial resistances of these different battery configurations. The $Li_3InCl_{5.5}F_{0.5}$-based battery displays the smallest interfacial resistances, while the $Li_{5.5}PS_{4.5}Cl_{1.5}$-based battery suffers the largest during cycling tests. *Ex-situ* TEM results verify that severe side reactions occur in the $LiNi_{0.7}Mn_{0.2}Co_{0.1}O_2$-$Li_{5.5}PS_{4.5}Cl_{1.5}$ cathode mixture during cycling, while good high voltage stable $LiInF_4$ phase and poor electrochemical stability $InCl_3$ phase are generated during cycling at higher upper cut-off voltages for $LiNi_{0.7}Mn_{0.2}Co_{0.1}O_2$-$Li_3InCl_{5.5}F_{0.5}$ and $LiNi_{0.7}Mn_{0.2}Co_{0.1}O_2$-$Li_3InCl_6$ cathodes, respectively. Additionally, the $Li_3InCl_{5.5}F_{0.5}$-based battery shows superior electrochemical performance when compared to the Li_3InCl_6-based battery at higher charge/discharge C-rates and even at a higher upper cut-off voltage (4.8 V *vs.* Li^+/Li^0). This study sheds a light on designing solid electrolytes with a wide voltage window to achieve high energy densities in ASSLBs when empolying high-voltage cathode materials.

Declaration of competing interest

The authors declare no competing financial interest.

Acknowledgments

This work was supported by the National Key Research and Development Program of China (No. 2021YFB2400300). We also thank the National Natural Science Foundation of China (Nos. 52177214, 22205153) for supporting our work. We gratefully acknowledge the Analytical and Testing Center of HUST and Soochow University for the technical support.

Supplementary materials

Supplementary material associated with this article can be found, in the online version, at doi:10.1016/j.cclet.2024.109741.

References

[1] S. Randau, D.A. Weber, O. Kötz, et al., Nat. Energy 5 (2020) 259–270.
[2] P. Adeli, J.D. Bazak, K.H. Park, et al., Angew. Chem. Int. Ed. 58 (2019) 8681–8686.
[3] T.K. Schwietert, V.A. Arszelewska, C. Wang, et al., Nat. Mater. 19 (2020) 428–435.
[4] H. Wan, B. Zhang, S. Liu, et al., Adv. Energy Mater. (2023) 2303046.
[5] Z. Jiang, C. Liu, C. Wei, et al., Ind. Eng. Chem. Res. 62 (2023) 21546–21557.
[6] H. Wan, Z. Wang, W. Zhang, et al., Nature 623 (2023) 739–744.
[7] L. Peng, S. Chen, C. Yu, et al., ACS Appl. Mater. Interfaces 14 (2022) 4179–4185.

[8] M. Yang, H. Li, F. Wu, Energy Mater. Adv. 2022 (2022) 41.
[9] N. Sun, Y. Song, Q. Liu, et al., Adv. Energy Mater. 12 (2022) 2200682.
[10] A. Zhang, J. Wang, R. Yu, et al., ACS Appl. Mater. Interfaces 15 (2023) 8190–8199.
[11] Z. Wang, C. Zhao, S. Sun, et al., Matter 6 (2023) 1096–1124.
[12] C. Yu, G. Li, X. Guan, et al., PCCP 14 (2012) 12368–12377.
[13] C. Wang, K. Fu, S.P. Kammampata, et al., Chem. Rev. 120 (2020) 4257–4300.
[14] Q. Guo, F. Xu, L. Shen, et al., Energy Mater. Adv. 2022 (2022) 8.
[15] C. Wei, X. Liu, C. Yu, et al., Chin. Chem. Lett. (2022) 107859.
[16] Q. Luo, L. Ming, D. Zhang, et al., Energy Mater. Adv. 4 (2023) 0065.
[17] L. Peng, C. Yu, C. Wei, et al., Acta Phys. Chim. Sin. 39 (2023) 2211034.
[18] L. Ming, D. Liu, Q. Luo, et al., Chin. Chem. Lett. (2023) 109087.
[19] T. Chen, D. Zeng, L. Zhang, et al., J. Energy Chem. 59 (2021) 530–537.
[20] S. Chen, C. Yu, C. Wei, et al., Energy Mater. Adv. 4 (2023) 1–10.
[21] X. Li, J. Liang, J. Luo, et al., Energy Environ. Sci. 12 (2019) 2671.
[22] S. Chen, C. Yu, Q. Luo, et al., Acta Phys. Chim. Sin. 39 (2023) 2210032.
[23] S. Chen, C. Yu, C. Wei, et al., Chin. Chem. Lett. 34 (2022) 107544.
[24] X. Luo, D. Cai, X. Wang, et al., ACS Appl. Mater. Interfaces 14 (2022) 29844–29855.
[25] L. Zhou, C. Kwok, A. Shyamsunder, et al., Energy Environ. Sci. 13 (2020) 2056–2063.
[26] T. Ma, Z. Wang, D. Wu, et al., Energy Environ. Sci. 16 (2023) 2142–2152.
[27] K. Wang, Q. Ren, Z. Gu, et al., Nat. Commun. 12 (2021) 4410.
[28] T. Asano, A. Sakai, S. Ouchi, et al., Adv. Mater. 30 (2018) 1803075.
[29] S. Wang, Q. Bai, A.M. Nolan, et al., Angew. Chem. Int. Ed. 58 (2019) 8039–8043.
[30] I. Kochetkov, T. Zuo, R. Ruess, et al., Energy Environ. Sci. 15 (2022) 3933.
[31] C. Wei, R. Wang, Z. Wu, et al., Chin. Chem. Lett. 35 (2024) 108717.
[32] C. Wei, R. Wang, Z. Wu, et al., Chem. Engin. J. 476 (2023) 146531.
[33] C. Yu, S. Ganapathy, E. van Eck, et al., J. Energy Chem. 38 (2019) 1–7.
[34] C. Wei, C. Liu, Y. Xiao, et al., Adv. Funct. Mater. 34 (2024) 2314306.
[35] C. Wei, S. Chen, C. Yu, et al., Appl. Mater. Today 31 (2023) 101770.
[36] Z. Jiang, C. Yu, S. Chen, et al., Scripta Mater. 227 (2023) 115303.
[37] Z. Jiang, S. Chen, C. Wei, et al., Chin. Chem. Lett. 35 (2024) 108561.
[38] X. Li, Q. Sun, Z. Wang, et al., J. Power Sources 456 (2020) 227997.
[39] Z. Chen, J. Meng, Y. Wang, et al., Electrochim. Acta 378 (2021) 138138.
[40] S. Zhang, F. Zhao, S. Wang, et al., Adv. Energy Mater. 11 (2021) 2100836.
[41] Y. Kim, S. Choi, J. Power Sources 567 (2023) 232962.
[42] X. Yang, Q. Yin, C. Wang, et al., Prog. Mater. Sci. 140 (2023) 101193.